LETTER

doi:10.1038/nature21053

Structural basis of co-translational quality control by ArfA and RF2 bound to ribosome

Fuxing Zeng[1], Yanbo Chen[1], Jonathan Remis[2], Mrinal Shekhar[3,4], James C. Phillips[4], Emad Tajkhorshid[1,3,4] & Hong Jin[1,3]

Quality control mechanisms intervene appropriately when defective translation events occur, in order to preserve the integrity of protein synthesis. Rescue of ribosomes translating on messenger RNAs that lack stop codons is one of the co-translational quality control pathways. In many bacteria, ArfA recognizes stalled ribosomes and recruits the release factor RF2, which catalyses the termination of protein synthesis[1–3]. Although an induced-fit mechanism of nonstop mRNA surveillance mediated by ArfA and RF2 has been reported[4], the molecular interaction between ArfA and RF2 in the ribosome that is responsible for the mechanism is unknown. Here we report an electron cryo-microscopy structure of ArfA and RF2 in complex with the 70S ribosome bound to a nonstop mRNA. The structure, which is consistent with our kinetic and biochemical data, reveals the molecular interactions that enable ArfA to specifically recruit RF2, not RF1, into the ribosome and to enable RF2 to release the truncated protein product in this co-translational quality control pathway. The positively charged C-terminal domain of ArfA anchors in the mRNA entry channel of the ribosome. Furthermore, binding of ArfA and RF2 induces conformational changes in the ribosomal decoding centre that are similar to those seen in other protein-involved decoding processes. Specific interactions between residues in the N-terminal domain of ArfA and RF2 help RF2 to adopt a catalytically competent conformation for peptide release. Our findings provide a framework for understanding recognition of the translational state of the ribosome by new proteins, and expand our knowledge of the decoding potential of the ribosome.

Elegant surveillance mechanisms have evolved to ensure that protein translation is error-free[5–7]. When a ribosome becomes involved in the translation of mRNAs that have no stop codons (nonstop translation), it is destined to stall at the end of the mRNA, unable to either elongate or terminate the nascent peptide chain because its aminoacyl site (A-site) is unoccupied. Bacteria are known to have three mechanisms for resolving stalled ribosomal complexes that result from nonstop translation, all of which start with recognition of truncated mRNAs and end with release of nascent polypeptides from the stalled ribosome[6,7].

One of these mechanisms, the ArfA/RF2-mediated surveillance pathway, involves ArfA[1–3] and a class I protein release factor, RF2, which catalyses peptide release during normal translational termination[8] and quality control[9]. Although the GGQ motif[10–12] in RF2 is required for peptide release in the pathway, the tripeptide SPF motif[8], which is essential for stop-codon recognition by RF2, appears to be dispensable[2]. Furthermore, nucleotides in the 16S ribosomal RNA (rRNA) that are close to ArfA when it binds to the ribosome have been identified[13].

Despite these developments, the molecular interactions that enable ArfA to recruit RF2 and help it to adopt its catalytically competent conformation remain unknown. Peptide release catalysed by ArfA and RF2 on a nonstop mRNA in the ribosome is achieved by an induced-fit mechanism[4], as seen in transfer RNA (tRNA) decoding on a sense codon[14] and canonical termination on a stop codon[15]. Here we report the molecular interactions responsible for the mechanism, as revealed by an electron cryo-microscopy (cryoEM) structure of the bacterial 70S ribosome bound to biologically related RF2, with its GGQ motif methylated[4], and ArfA[16,17], reconstructed to an overall resolution of 3.52 Å (Fig. 1, Extended Data Figs 1 and 2 Extended Data Table 1). The functional importance of these molecular interactions is further supported by results from real-time kinetic experiments (Extended Data Table 2).

As expected[4], the ribosome is in a non-rotated state (Fig. 1a, b), and the 30S subunit is in a 'closed' conformation[18]. The overall conformation of RF2 in the ribosome is similar to that reported on canonical termination complexes for stop-codon recognition[19–22] (Extended Data Fig. 3). ArfA adopts an extended conformation and interacts across the subunit interface of the ribosome reaching from the mRNA entry channel, across the decoding centre, to the 'B2a bridge', the subunit junction that is formed by helix 69 of 23S rRNA (H69) and helix 44 of 16S rRNA (h44) in the ribosome (Fig. 1c).

The positively charged C-terminal region of ArfA (residues 33–44) inserts into the mRNA entry channel downstream of the A-site. Its highly conserved R41 and an upstream KGKG motif (residues 34–37; Extended Data Fig. 4a) interact with the phosphate backbone of the 16S rRNA, which forms the mRNA entry channel (Fig. 2a and Extended Data Fig. 5a, b), anchoring the protein in the subunit interface of the ribosome. Although the length and amino acid sequence of the C-terminal tail of ArfA vary among species, they all contain positively charged amino acids (Extended Data Fig. 4b). Furthermore, similar interactions have been reported in the other two nonstop ribosomal complexes[23,24]. Together, these observations suggest that proteins that are recruited to a ribosome stalled on a truncated mRNA recognize an empty ribosomal mRNA entry channel mainly via electrostatic interactions.

ArfA detects the presence of an empty A-site in the ribosome. Residues P23–E30 of ArfA interact with the ribosomal decoding centre (Fig. 2b and Extended Data Fig. 5c). Conformational flexibility conferred by loop 3 of ArfA (Extended Data Fig. 4a) and the 3′-end of the truncated mRNA in this region probably allows ArfA to accommodate one to two codons in the mRNA downstream from the ribosomal P-site (Extended Data Fig. 5d), consistent with the results of biochemical experiments[1,4,13]. Binding of ArfA and RF2 to the ribosome induces conformational changes in the decoding centre. One of the two bases essential for decoding in h44, A1492 and A1493, stacks on A1913 of H69 in the 23S rRNA, a feature of the ribosomal decoding centre that has been seen repeatedly when proteins 'decode' the state of the A-site in the ribosome[22–26]. A1492 is modelled to stack with A1913, and the base of A1493 appears to be disordered and is refined to a conformation that is flipped out of h44. A proline residue (P23) of ArfA stacks on A1492 (Fig. 2b). A P23A mutation decreases the catalytic constant (k_{cat}) of the peptide release reaction by about half (Fig. 2c and Extended Data Fig. 6a), suggesting that the interaction between this proline and

[1]Department of Biochemistry, University of Illinois at Urbana-Champaign, Urbana, Illinois 61801, USA. [2]Department of Molecular Biosciences, Northwestern University, Evanston, Illinois 60208-3500, USA. [3]Center for Biophysics and Quantitative Biology, University of Illinois at Urbana-Champaign, Urbana, Illinois 61801, USA. [4]Beckman Institute for Advanced Science and Technology, University of Illinois at Urbana-Champaign, Urbana, Illinois 61801, USA.

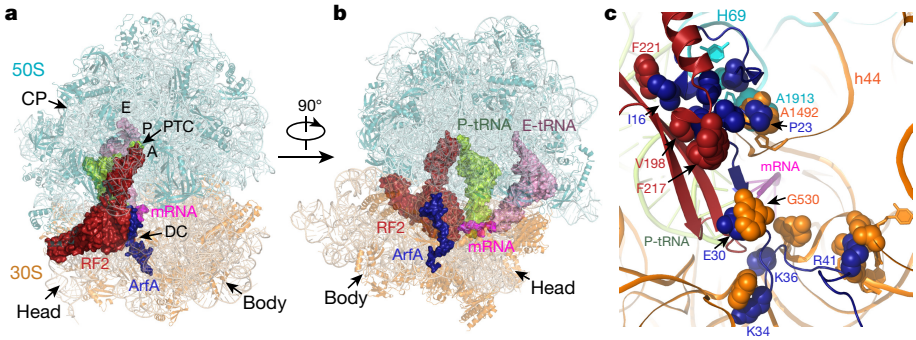

Figure 1 | Structure of ArfA and RF2 bound to the ribosome on a nonstop mRNA. a, **b**, Overall view of the ribosomal nonstop complex shows the structure of the 70S ribosome in complex with $tRNA^{fMet}$ in the exit (E) and peptidyl (P) sites, a nonstop mRNA, and ArfA and RF2 in the A-site. ArfA (density), RF2 (firebrick), P-tRNA (lemon), E-tRNA (pink) and a nonstop mRNA (magenta) are shown in surface representation. Ribosomal RNA and proteins are shown as cartoons. CP, central protuberance; DC, decoding centre. **c**, Overview of ArfA in the ribosome as seen from the mRNA entry channel. Contacts between ArfA and RF2 with the ribosome are shown as spheres.

rRNA is functionally important, probably stabilizing the A–A stacking and helping to establish a connection between the mRNA entry channel and the conformational state of 23S rRNA in the large subunit of the ribosome.

By contrast, although E30 of ArfA stacks with G530 of h18 of the 16S rRNA, an E30A mutation causes little change in the value of k_{cat} of the release reaction (Fig. 2c). Furthermore, as seen in the C-terminal tail of ArfA, electrostatic interactions between ArfA and rRNA are observed in this region (Extended Data Fig. 5c). However, single amino acid mutations of conserved positively charged residues in ArfA from R26 to R41 only marginally affect the kinetics of the peptide release reaction catalysed by RF2 (Fig. 2c and Extended Data Fig. 6a–c), suggesting redundancy of the electrostatic interactions between the rRNA and the C-terminal domain of ArfA in the pathway.

Notably, the SPF tripeptide motif[8] in RF2 'falls' into the decoding pocket, but it does not interact with ArfA or with the three essential nucleotides in the 16S rRNA, which are more than 5 Å away. This observation not only explains why the SPF motif is functionally dispensable, but also suggests that ArfA is responsible for detecting the presence of an empty A-site in the nonstop stalled ribosome.

Sequence-specific interactions between ArfA and RF2 explain why only RF2 is recruited. Residues 27–29 in ArfA form a β-sheet (β1) anti-parallel to β5 in the region from residues 214–216 in domain II of RF2 (Fig. 2b). Extensive hydrophobic interactions are observed between residues in the α2 to loop 2 regions of ArfA and β4 and β5 in domain II of RF2. The hydrophobic side chains of L19, L20, L24 and F25 in ArfA form a unique hydrophobic surface that packs with V198 and F217 of RF2 on one side, and with W319 of RF2 on the other (Fig. 2d). W319 resides in the so-called switch loop[25] that has been suggested to be important for peptide release by protein release factors. It is likely that the packing of W319 with the hydrophobic surface of ArfA stabilizes the switch loop, thereby facilitating the catalytic function of RF2 for peptide release. By contrast, RF1 cannot form similar hydrophobic interactions with ArfA, because it does not contain amino acids with bulky hydrophobic side chains at the equivalent positions of 198, 217 and 319 (Extended Data Fig. 7). Thus, the differences in sequence between the two release factors in this region explain why RF2, rather than RF1, is recruited into the ribosome by ArfA.

The N-terminal domain of ArfA forms a tight helix and turn conformation that is nicely sandwiched between the α7 helix in RF2 and the interface of the 23S and 16S rRNAs (Fig. 3a, b), and this region is important for stabilizing the catalytically competent conformation of RF2 for the peptide release in the ribosome. Positively charged K8

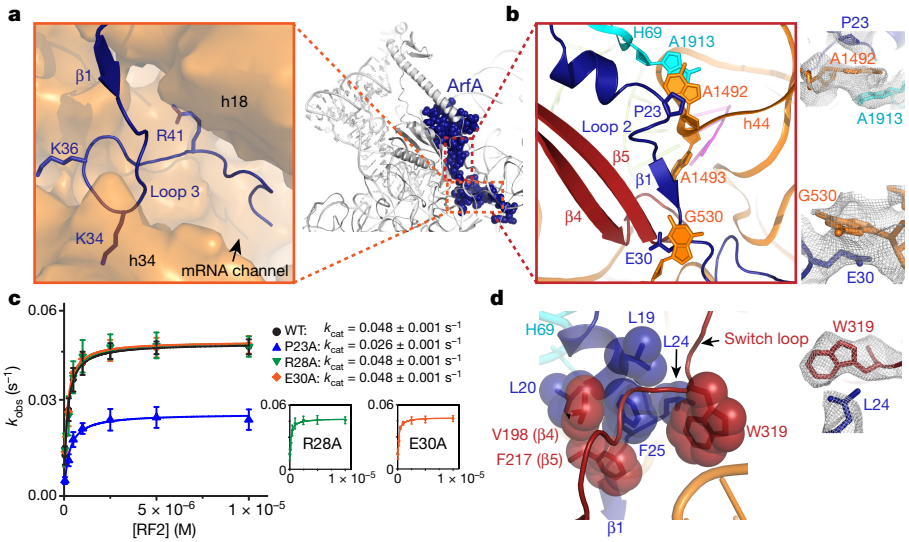

Figure 2 | Interactions between ArfA and RF2 in the ribosome. a, The positively charged C-terminal tail of ArfA occupies the empty mRNA channel (surface, orange). **b**, Binding of ArfA and RF2 in the ribosomal A-site. **c**, Observed rate versus RF2 concentrations showing fits for the k_{cat} and $K_{1/2}$ calculations for wild-type ArfA, and P23A, R28A and E30A mutants. k_{cat}, catalytic rate constant; $K_{1/2}$, the RF2 concentration at which half of the maximal rate is achieved; k_{obs}, observed rate. An average of three independent measurements is reported for each reaction and errors are calculated by standard error propagation. **d**, Hydrophobic interactions important for the recruitment of RF2 by ArfA in the ribosome. Electron microscopy maps of important interactions are shown. ArfA, density; RF2, firebrick; 16S rRNA, orange; 23S rRNA, cyan.

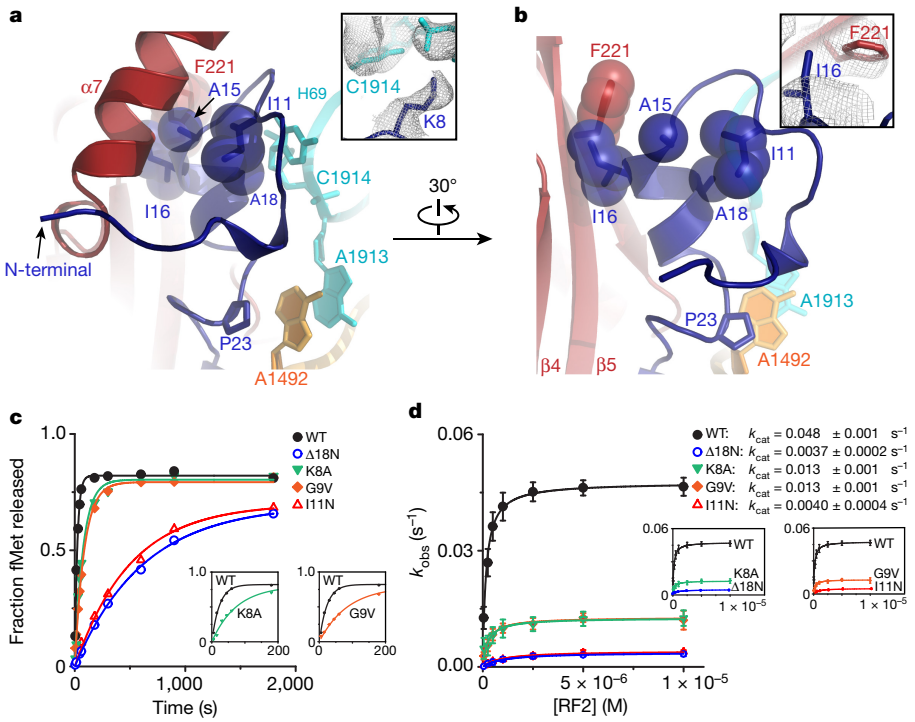

Figure 3 | The activation domain of ArfA. a, **b**, The N-terminal domain of ArfA packs with α7 of RF2 and the B2a bridge between h44 and H69 in the ribosome. In **b**, α7 is removed to show the interaction between I16 in ArfA (density) and F221 in RF2 (firebrick). **c**, Representative time courses of peptide release at 25 nM nonstop ribosomal complexes by 5 μM RF2 with 62.5 nM wild-type and mutant ArfA proteins. **d**, Observed rate versus RF2 concentrations showing fits for catalytic rate constant k_{cat} and $K_{1/2}$ calculations for wild-type ArfA and mutant ArfA proteins. These mutants are an N-terminal 18 amino acids truncated ArfA (Δ18N), K8A, G9V and I11N. An average of three independent measurements is reported for each reaction and errors are calculated by standard error propagation.

interacts with the phosphate backbone of C1914 in H69 (Fig. 3a). Contrary to the redundant electrostatic interactions observed in the C-terminal domain of ArfA, a K8A mutation compromises the peptide release activity in the ribosome (Fig. 3c, d). Furthermore, a highly conserved G9 introduces a sharp turn of the backbone in this region. The conformation of the loop is stabilized by extensive hydrophobic interactions among the highly conserved residues I11, A15 and A18 (Fig. 3b). A disruption of the G9-introduced turn or of the hydrophobic interactions in the loop severely compromises the peptide release activity of RF2 (Fig. 3c, d and Extended Data Fig. 6d). Notably, the effects on the kinetics of the release reaction are nearly the same for the ArfA mutants with a I11N point mutation and with a truncation of the N-terminal 18 amino acids.

An isoleucine residue at position of 16 in ArfA (I16) at the junction of the loop and the helix forms hydrophobic interactions with F221 in β5 of RF2 (Fig. 3b). This hydrophobic interaction is likely to be important for inducing RF2 into a catalytically competent conformation, because RF2 from *Thermus thermophilus*, which contains a glutamic acid (E) at the equivalent position of 221 but otherwise the same amino acids at the equivalent positions of 198, 217 and 319, can bind to the

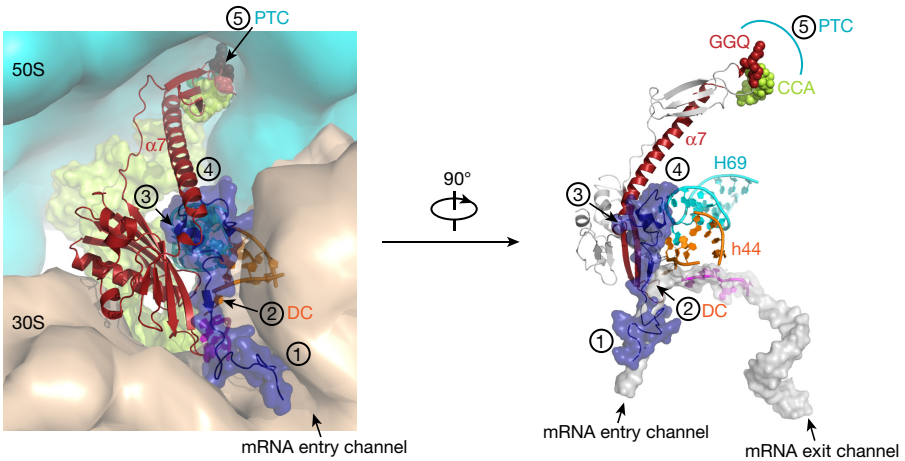

Figure 4 | Schematic representation of sequential events involved in rescuing a nonstop translation by ArfA and RF2 in the ribosome. 1, Sensing and anchoring. The positively charged C-terminal domain of ArfA senses an empty mRNA channel in the ribosome, where a highly conserved R41 and KGKG motif anchor the ArfA tail into the mRNA entry channel. 2, Detecting the translational state. Relatively flexible loop regions in ArfA detect the presence of an empty ribosomal A site. 3, Recruiting RF2. Sequence-specific hydrophobic interactions in the N-terminal domain of ArfA recruit RF2. 4, Activation. The N-terminal helix and turn conformation mediated by hydrophobic interactions in ArfA and other interactions including I16 of ArfA and F221 of RF2 help to induce RF2 to adopt a catalytically competent conformation, docking the GGQ motif into the PTC in the large ribosomal subunit. 5, Peptide release.

ribosome (Extended Data Fig. 8a) but fails to catalyse the peptide release reaction (Extended Data Fig. 8b).

Together, these results suggest that the molecular interactions observed between the N-terminal domain of ArfA and RF2 are important for positioning RF2 in a catalytic-competent form, and for docking the universally conserved GGQ motif into the peptidyl transferase centre (PTC) of the ribosome. The PTC of the ribosome is in a fully induced state[26,27], primed for the release of the nascent peptide in the ribosome.

In conclusion, our combined structural and biochemical investigation demonstrates how a rescuing signal generated by proteins down in the mRNA entry channel is transmitted over approximately 80 Å to the PTC of the large ribosomal subunit, where the elongation of a nascent peptide chain is terminated (Fig. 4). The observation that a small protein such as ArfA can be recruited to facilitate the function of a release factor in terminating protein synthesis in the ribosome suggests a new way of regulating translation that can be used in the development of antibacterial and antigrowth therapeutic agents that target the translating ribosome.

Online Content Methods, along with any additional Extended Data display items and Source Data, are available in the online version of the paper; references unique to these sections appear only in the online paper.

Received 21 October; accepted 14 December 2016.
Published online 11 January 2017.

1. Shimizu, Y. ArfA recruits RF2 into stalled ribosomes. *J. Mol. Biol.* **423,** 624–631 (2012).
2. Chadani, Y., Ito, K., Kutsukake, K. & Abo, T. ArfA recruits release factor 2 to rescue stalled ribosomes by peptidyl-tRNA hydrolysis in *Escherichia coli*. *Mol. Microbiol.* **86,** 37–50 (2012).
3. Chadani, Y. *et al.* Ribosome rescue by *Escherichia coli* ArfA (YhdL) in the absence of trans-translation system. *Mol. Microbiol*. **78,** 796–808 (2010).
4. Zeng, F. & Jin, H. Peptide release promoted by methylated RF2 and ArfA in nonstop translation is achieved by an induced-fit mechanism. *RNA* **22,** 49–60 (2016).
5. Rodnina, M. V. Quality control of mRNA decoding on the bacterial ribosome. *Adv. Protein Chem. Struct. Biol*. **86,** 95–128 (2012).
6. Keiler, K. C. Mechanisms of ribosome rescue in bacteria. *Nat. Rev. Microbiol.* **13,** 285–297 (2015).
7. Giudice, E. & Gillet, R. The task force that rescues stalled ribosomes in bacteria. *Trends Biochem. Sci.* **38,** 403–411 (2013).
8. Ito, K., Uno, M. & Nakamura, Y. A tripeptide 'anticodon' deciphers stop codons in messenger RNA. *Nature* **403,** 680–684 (2000).
9. Zaher, H. S. & Green, R. Quality control by the ribosome following peptide bond formation. *Nature* **457,** 161–166 (2009).
10. Frolova, L. Y. *et al.* Mutations in the highly conserved GGQ motif of class 1 polypeptide release factors abolish ability of human eRF1 to trigger peptidyl-tRNA hydrolysis. *RNA* **5,** 1014–1020 (1999).
11. Mora, L. *et al.* The essential role of the invariant GGQ motif in the function and stability *in vivo* of bacterial release factors RF1 and RF2. *Mol. Microbiol.* **47,** 267–275 (2003).
12. Dinçbas-Renqvist, V. *et al.* A post-translational modification in the GGQ motif of RF2 from *Escherichia coli* stimulates termination of translation. *EMBO J.* **19,** 6900–6907 (2000).
13. Kurita, D., Chadani, Y., Muto, A., Abo, T. & Himeno, H. ArfA recognizes the lack of mRNA in the mRNA channel after RF2 binding for ribosome rescue. *Nucleic Acids Res.* **42,** 13339–13352 (2014).
14. Rodnina, M. V., Beringer, M. & Wintermeyer, W. Mechanism of peptide bond formation on the ribosome. *Q. Rev. Biophys.* **39,** 203–225 (2006).
15. Youngman, E. M., He, S. L., Nikstad, L. J. & Green, R. Stop codon recognition by release factors induces structural rearrangement of the ribosomal decoding center that is productive for peptide release. *Mol. Cell* **28,** 533–543 (2007).
16. Garza-Sánchez, F., Schaub, R. E., Janssen, B. D. & Hayes, C. S. tmRNA regulates synthesis of the ArfA ribosome rescue factor. *Mol. Microbiol*. **80,** 1204–1219 (2011).
17. Schaub, R. E., Poole, S. J., Garza-Sánchez, F., Benbow, S. & Hayes, C. S. Proteobacterial ArfA peptides are synthesized from nonstop messenger RNAs. *J. Biol. Chem.* **287,** 29765–29775 (2012).
18. Ogle, J. M., Murphy, F. V., Tarry, M. J. & Ramakrishnan, V. Selection of tRNA by the ribosome requires a transition from an open to a closed form. *Cell* **111,** 721–732 (2002).
19. Klaholz, B. P. *et al.* Structure of the *Escherichia coli* ribosomal termination complex with release factor 2. *Nature* **421,** 90–94 (2003).
20. Korostelev, A. *et al.* Crystal structure of a translation termination complex formed with release factor RF2. *Proc. Natl Acad. Sci. USA* **105,** 19684–19689 (2008).
21. Rawat, U. B. S. *et al.* A cryo-electron microscopic study of ribosome-bound termination factor RF2. *Nature* **421,** 87–90 (2003).
22. Weixlbaumer, A. *et al.* Insights into translational termination from the structure of RF2 bound to the ribosome. *Science* **322,** 953–956 (2008).
23. Gagnon, M. G., Seetharaman, S. V., Bulkley, D. & Steitz, T. A. Structural basis for the rescue of stalled ribosomes: structure of YaeJ bound to the ribosome. *Science* **335,** 1370–1372 (2012).
24. Neubauer, C., Gillet, R., Kelley, A. C. & Ramakrishnan, V. Decoding in the absence of a codon by tmRNA and SmpB in the ribosome. *Science* **335,** 1366–1369 (2012).
25. Laurberg, M. *et al.* Structural basis for translation termination on the 70S ribosome. *Nature* **454,** 852–857 (2008).
26. Jin, H., Kelley, A. C., Loakes, D. & Ramakrishnan, V. Structure of the 70S ribosome bound to release factor 2 and a substrate analog provides insights into catalysis of peptide release. *Proc. Natl Acad. Sci. USA* **107,** 8593–8598 (2010).
27. Schmeing, T. M., Huang, K. S., Strobel, S. A. & Steitz, T. A. An induced-fit mechanism to promote peptide bond formation and exclude hydrolysis of peptidyl-tRNA. *Nature* **438,** 520–524 (2005).

Acknowledgements We thank J. Peng for scripting, W. Jiang, Y. He, J. Liu and T. H. D. Nguyen for suggestions on EM data collection and structural refinement, members of the Jin laboratory for discussions, the structural biology facility at Northwestern University for the use of the microscope and the Chicago Biomedical Consortium for the purchase of the Gatan K2 detector. H.J. acknowledges support from the National Institute of General Medical Sciences of the NIH (R01-GM120552). The computational part of the study was supported by the National Institute of General Medical Sciences (P41-GM104601 to J.C.P. and E.T.).

Author Contributions F.Z. and H.J. designed the study. F.Z. purified ribosomes, proteins and tRNAs, processed EM data and built the atomic model. Y.C. did the mutagenesis and purified ArfA mutants. F.Z. and Y.C. performed the peptide release assay. F.Z., Y.C., H.J. and J.R. collected EM data. M.S., J.C.P. and E.T. provided computational support. F.Z., Y.C. and H.J. analysed the data and refined the structure. F.Z. and Y.C. helped with manuscript preparation. H.J. wrote the paper. All authors discussed the final manuscript.

Author Information Reprints and permissions information is available at www.nature.com/reprints. The authors declare no competing financial interests. Readers are welcome to comment on the online version of the paper. Correspondence and requests for materials should be addressed to H.J. (hjin@illinois.edu).

Reviewer Information *Nature* thanks Y. Hashem, K. Keiler and the other anonymous reviewer(s) for their contribution to the peer review of this work.

METHODS

Preparation of *Escherichia coli* ribosomes, tRNAs and initiation factors. 70S ribosomes from *E. coli* MRE600 strain[28] were prepared as described[29]. ArfA, RF2 and $tRNA^{fMet}$ were cloned from *E. coli* K12 strain[30] and were purified[4]. *E. coli* IF1, IF2, and IF3 were overexpressed and purified[31]. The mRNA with the sequence 5′-GGC AAG GAG GUA AAA AUG-3′ (P-site underlined) was purchased from Dharmacon (Amersham/GE Healthcare).

Purification of the two biologically related proteins ArfAΔ17C and RF2 with fully methylated GGQ^m motif. The expression of the full-length *E. coli* ArfA and ArfA-homologue proteins from other bacterial species is regulated by RNases and tmRNA–SmpB activity. In the absence of the tmRNA–SmpB system, the C-terminal 17 amino acid truncated protein ArfAΔ17C is produced by RNase III in *E.coli*, and is used to recruit RF2 to rescue the stalled ribosome[16,17,32]. Furthermore, the glutamine of the universally conserved GGQ motif[10,11] in RF2 is methylated (GGQ^m)[12]. This conserved post-translational modification stimulates the catalytic function of RF2 tenfold *in vitro*[4] and is functionally important *in vivo*. Thus, the two biologically related proteins, ArfAΔ17C and RF2 with the GGQ^m motif, are used in this study and are referred to as ArfA and RF2, respectively, for clarity. Point mutations in ArfA were generated by mutagenesis and mutant ArfA proteins were purified in the same way as wild-type ArfA[4].

Preparation of charged $tRNA^{fMet}$. *E. coli* methionine-tRNA synthetase (MetRS) and methionyl-tRNA formyltransferase (FMT) were purified[33]. Aminoacylation and formylation of $tRNA^{fMet}$ were performed as described previously[4,34]. Briefly, 20 μM $tRNA^{fMet}$ was incubated with 0.6 mM L-methionine, 1 μM L-[^{35}S]-methionine (PerkinElmer), 0.6 mM 10-formyltetrahydrofolate, 12 μM MetRS, 12 μM FMT, 10 mM ATP, and 0.02 U/μl pyrophosphatase at 37 °C for 40 min in a buffer containing 100 mM HEPES-KOH, pH 7.6, 20 mM KCl, 10 mM $MgCl_2$ and 1 mM DTT. Charged fMet-$tRNA^{fMet}$ was purified by phenol:chloroform extraction followed by ethanol precipitation and stored in 2 mM NaOAc, pH 5.2.

Peptide release assay. The k_{cat} and $K_{1/2}$ of peptide release were measured as described[4]. The release complex was first formed by incubating ribosome (2 μM), mRNA (6 μM), IF1, IF2, IF3 (3 μM each), fMet-$tRNA^{fMet}$ (3 μM) and GTP (2 mM) at 37 °C for 30 min in buffer containing 50 mM Tris, pH 7.4, 70 mM NH_4Cl, 30 mM KCl, 10 mM $MgCl_2$ and 5 mM β-mercaptoethanol. The complex was purified by sucrose cushion. 25 nM release complexes were then reacted with 62.5 nM ArfA and RF2 with concentrations of 50 nM–30 μM at 37 °C for between 1 s and 30 min. The reactions were stopped by adding 5% ice-cold trichloroacetic acid and spun at 18,000 *g* for 10 min at 4 °C. The supernatant with released f-[^{35}S]-Met was counted using ScintiSafe Econo 1 Cocktail (Fisher Scientific). The maximally releasable fMet ($fMet_{Max}$) was measured by incubating 25 nM release complex with 100 μM puromycin (Sigma-Aldrich) at 37 °C for 30 s. The background level of released fMet in the absence of RF2 was measured at the same time points. The fraction of released fMet (the ratio between the released f-[^{35}S]-Met and $fMet_{Max}$) against time was plotted and fitted to $F_t = F_{max}(1 - e^{-k_{obs}t})$. k_{cat} and $K_{1/2}$ were obtained by plotting k_{obs} against the concentration of RF2 and fitting with $k_{obs} = k_{cat}[RF2]/(K_{1/2} + [RF2])$.

Formation of heterologous release complexes comprised of *E. coli* ribosome and *T. thermophilus* RF2. *T. thermophilus* RF2 was co-expressed with its cognate methyltransferase in the *E. coli* BL21 (DE3) strain[35] to achieve full methylation of the GGQ motif, and the resulting protein was purified as described previously[4]. To form heterogolous nonstop ribosomal complexes, 50 μl *E. coli* 70S ribosome (4 μM), mRNA (8 μM), $tRNA^{fMet}$, *E. coli* ArfA and *T. thermophilus* RF2 (16 μM each) were incubated at 37 °C for 30 min. The unbound factors were removed by size-exclusion chromatography using a Superdex 200 (10/30) column (Amersham/GE Healthcare). The ribosomal complex peak was collected and the binding of *T. thermophilus* RF2 to the *E. coli* ribosome was confirmed by SDS–PAGE.

Electron microscopy and image processing. Ribosomal complexes were formed by incubating ribosomes with mRNA, $tRNA^{fMet}$, ArfA and RF2 together at 37 °C in a buffer containing 20 mM Hepes-KOH, pH 7.5, 15 mM magnesium acetate, 150 mM potassium acetate, 4 mM β-mercapthoethanol, 2 mM spermidine and 0.05 mM spermin[36].

Sample preparation for cryoEM was done as described[37,38]. Aliquots of 2 μl nonstop ribosomal complex were incubated for 30 s on glow-discharged holey carbon grids with thin-layer carbon film (C-Flat TM Holey Carbon Grid CF-2/0.5-4C, 400 mesh, Copper, Protochips). Grids were blotted for 3.5 s in 100% humidity at 4 °C and plunge frozen with a Vitrobot Mark IV (FEI). Data were collected in vitreous ice using a JEOL 3200 FS transmission electron microscope operating at 300 keV. A total of 3,482 micrographs were acquired with a K2 summit direct electron detector (Gatan) operating in super mode at a calibrated magnification of 83,822× (0.5965 Å per pixel) using a defocus range of −0.7 to −3 μm and a dose of 20 e^- $Å^{-2}$. Each micrograph was acquired as a 30-frame movie during a 6-s exposure. Movie frames were aligned using MotionCor2 to correct beam-induced motion and drift[39], and the aligned images were summed for further image processing. The contrast transfer function (CTF) was estimated using CTFFIND4[40]. All subsequent processing steps were performed in Relion[41–43].

Ribosome particles were picked using a semi-automated particle picking procedure[44], after which micrographs were inspected individually. Micrographs with improper defocus, ice contamination or poor CTF estimation were discarded. A total of 445,164 particles were extracted from the 2,748 micrographs and were subjected to reference-free 2D and 3D classifications in which non-ribosomal particles and particles for 50S and 30S were discarded. Statistical particle-based movie correction and radiation-damage weighing were performed[45] and the polished final 155,440 particles were subject to 3D refinement to yield a reconstruction at 3.52 Å.

Global, focused and local refinement. In global classification and refinement, a 3D classification of the 155,440 particles for the entire ribosome with a finer angular sampling of 1.8° and a local angular search range of 10° were performed, which led to two classes with different degrees of rotation of the 30S relative to the 50S subunit. The subsequent 3D refinement of these two classes yielded reconstructions of the nonstop complexes at 3.52 Å and 3.63 Å resolution, respectively (Extended Data Figs 1c, d, 2a). Coupled with the global domain movements observed in the ribosome, the binding ligands including a nonstop mRNA, E-tRNA, ArfA and RF2 all show different degrees of displacement. Despite these differences, based on the reconstructions obtained from the two classes, binding of ArfA and RF2 in the ribosomal A site induces the same conformational changes in the decoding centre of the ribosome. The 30S subunit adopts a closed conformation, and the CCA-end of the P-tRNA and the GGQ motif of RF2 are placed at the core of the PTC.

However, using the global classification and refinement procedure, the local resolution around the ArfA and RF2 region was estimated as 4–4.5 Å by ResMap[46] (Extended Data Fig. 2c). To obtain a higher resolution and a better resolved map of this region, we performed focused classification with or without signal subtraction[47–49] using masks over ArfA and RF2 (Extended Data Figs 1c, 2d, f).

First, focused 3D classifications with a mask over ArfA and RF2 (ArfA/RF2), or a mask over ArfA, RF2 and the 30S body domain (ArfA/RF2/30S body domain), were performed without orientational searches. This procedure led to one class from a total of 155,440 particles and a subsequent refinement of the particles in the class yielded reconstructions with an overall resolution at 4.5 Å and 3.7 Å, for masks over ArfA/RF2 and ArfA/RF2/30S body, respectively (Extended Data Figs 1c, 2d, e). Second, local refinements with signal subtraction over regions around ArfA/RF2 and ArfA/RF2/30S body were performed, which led to reconstructions with an overall resolution at 3.7 Å for the mask over ArfA/RF2, and 3.6 Å for the mask over ArfA/RF2/30S body domain (Extended Data Figs 1c, 2f–h).

The resolution was reported on the basis of the gold-standard Fourier shell correlation FSC = 0.143 criterion, after applying a soft spherical mask on the two reconstructions refined from the half of the data set independently[50]. Local resolution was estimated using ResMap[46].

Model building. Maps obtained from local refinements were used first for building the structure of ArfA in the ribosome. Homology models generated by Phyre2[51] and I-TASSER[52] were used as an intial guide, and regions of ArfA containing residues 8–14 and 24–37 were built *de novo* according to the electron microscopy map.

The ArfA structure thus built was fit as a rigid body into the overall map of the entire ribosomal nonstop complex. To build the ribosome structure, the high-resolution crystal structure of the *E. coli* ribosome (PDB: 4YBB)[53] was used and fit into the map using Chimera[54]. The body, head and shoulder domains of 30S were fit separately. Subsequently, H69, H25, H43, H77 and H84 of 23S rRNA, 5S rRNA, h44 of 16S rRNA and most of ribosomal proteins were fit into the map individually. A homology model of *E. coli* RF2 was generated using SWISS-MODEL[55] from *T. thermophilus* RF2 (PDB: 4V5J)[26]. The switch loop of RF2[25] was built according to the map obtained from local refinement. Model building was done in COOT[56].

Model refinement and validation. The model was refined using Refmac5.8[57] with secondary structure, RNA base-pair, sugar pucker and base stacking restraints generated by ProSMART[58] and LIBG[59]. The refinement weight was experimentally optimized in Refmac to balance the overall fit of the model to the map and the geometry of the structural model. Cross-validation of two half maps was done where FSC was monitored. The final model was validated using MolProbity[60]. Extended Data Table 1 summarizes refinement statistics for the overall and local structures. Maps were visualized using Chimera and figures were generated using PyMOL[61] and Chimera.

Data availability. Electron microscopy maps have been deposited in the Electron Microscopy Data Bank under accession codes EMD-8505 for the entire nonstop complex and EMD-8506 for the map around ArfA region. Coordinates have been deposited in the Protein Data Bank under accession codes 5U4I for the entire ribosomal complex and 5U4J for the coordinate around the ArfA region.

28. Cammack, K. A. & Wade, H. E. The sedimentation behaviour of ribonuclease-active and -inactive ribosomes from bacteria. *Biochem. J.* **96,** 671–680 (1965).
29. Bommer, U. *et al.* in *Subcellular Fractionation: A Practical Approach* (eds Graham, J. & Rickwood, D.) 271–301 (IRL, Washington, 1997).
30. Kurylo, C. M. *et al.* Genome sequence and analysis of *Escherichia coli* MRE600, a colicinogenic, nonmotile strain that lacks RNase I and the type I methyltransferase, EcoKI. *Genome Biol. Evol.* **8,** 742–752 (2016).
31. Wolfrum, A., Brock, S., Mac, T. & Grillenbeck, N. Expression in *E. coli* and purification of *Thermus thermophilus* translation initiation factors IF1 and IF3. *Protein Expr. Purif.* **29,** 15–23 (2003).
32. Chadani, Y. *et al.* Trans-translation-mediated tight regulation of the expression of the alternative ribosome-rescue factor ArfA in *Escherichia coli*. *Genes Genet. Syst.* **86,** 151–163 (2011).
33. Schmitt, E. *et al.* Crystallization and preliminary X-ray analysis of *Escherichia coli* methionyl-tRNA(fMet) formyltransferase. *Proteins* **25,** 139–141 (1996).
34. Walker, S. E. & Fredrick, K. Preparation and evaluation of acylated tRNAs. *Methods* **44,** 81–86 (2008).
35. Monteiro, R. A., Souza, E. M., Yates, M. G., Pedrosa, F. O. & Chubatsu, L. S. Use of lactose to induce expression of soluble NifA protein domains of *Herbaspirillum seropedicae* in *Escherichia coli*. *Can. J. Microbiol.* **46,** 1087–1090 (2000).
36. Sprink, T. *et al.* Structures of ribosome-bound initiation factor 2 reveal the mechanism of subunit association. *Sci. Adv.* **2,** e1501502 (2016).
37. Stark, H. & Chari, A. Sample preparation of biological macromolecular assemblies for the determination of high-resolution structures by cryo-electron microscopy. *Microscopy* **65,** 23–34 (2015).
38. Grassucci, R. A., Taylor, D. J. & Frank, J. Preparation of macromolecular complexes for cryo-electron microscopy. *Nat. Protocols* **2,** 3239–3246 (2007).
39. Li, X. *et al.* Electron counting and beam-induced motion correction enable near-atomic-resolution single-particle cryo-EM. *Nat. Methods* **10,** 584–590 (2013).
40. Rohou, A. & Grigorieff, N. CTFFIND4: Fast and accurate defocus estimation from electron micrographs. *J. Struct. Biol.* **192,** 216–221 (2015).
41. Scheres, S. H. A Bayesian view on cryo-EM structure determination. *J. Mol. Biol.* **415,** 406–418 (2012).
42. Scheres, S. H. RELION: implementation of a Bayesian approach to cryo-EM structure determination. *J. Struct. Biol.* **180,** 519–530 (2012).
43. Kimanius, D., Forsberg, B. O., Scheres, S. H. W. & Lindahl, E. Accelerated cryo-EM structure determination with parallelisation using GPUs in RELION-2. *eLife* **5,** e18722 (2016).
44. Scheres, S. H. Semi-automated selection of cryo-EM particles in RELION-1.3. *J. Struct. Biol.* **189,** 114–122 (2015).
45. Scheres, S. H. W. Beam-induced motion correction for sub-megadalton cryo-EM particles. *eLife* **3,** e03665 (2014).
46. Kucukelbir, A., Sigworth, F. J. & Tagare, H. D. Quantifying the local resolution of cryo-EM density maps. *Nat. Methods* **11,** 63–65 (2014).
47. Bai, X. C., Rajendra, E., Yang, G., Shi, Y. & Scheres, S. H. Sampling the conformational space of the catalytic subunit of human γ-secretase. *eLife* **4,** e11182 (2015)
48. Scheres, S. H. W. Processing of structurally heterogeneous cryo-EM data in RELION. *Methods Enzymol.* **579,** 125–157 (2016).
49. Nguyen, T. H. D. *et al.* Cryo-EM structure of the yeast U4/U6.U5 tri-snRNP at 3.7 Å resolution. *Nature* **530,** 298–302 (2016).
50. Scheres, S. H. & Chen, S. Prevention of overfitting in cryo-EM structure determination. *Nat. Methods* **9,** 853–854 (2012).
51. Kelley, L. A., Mezulis, S., Yates, C. M., Wass, M. N. & Sternberg, M. J. E. The Phyre2 web portal for protein modeling, prediction and analysis. *Nat. Protocols* **10,** 845–858 (2015).
52. Zhang, Y. I-TASSER server for protein 3D structure prediction. *BMC Bioinformatics* **9,** 40 (2008).
53. Noeske, J. *et al.* High-resolution structure of the *Escherichia coli* ribosome. *Nat. Struct. Mol. Biol.* **22,** 336–341 (2015).
54. Pettersen, E. F. *et al.* UCSF Chimera–a visualization system for exploratory research and analysis. *J. Comput. Chem.* **25,** 1605–1612 (2004).
55. Biasini, M. *et al.* SWISS-MODEL: modelling protein tertiary and quaternary structure using evolutionary information. *Nucleic Acids Res.* **42,** W252–W258 (2014).
56. Emsley, P., Lohkamp, B., Scott, W. G. & Cowtan, K. Features and development of Coot. *Acta Crystallogr. D* **66,** 486–501 (2010).
57. Murshudov, G. N. *et al.* REFMAC5 for the refinement of macromolecular crystal structures. *Acta Crystallogr. D* **67,** 355–367 (2011).
58. Nicholls, R. A., Fischer, M., McNicholas, S. & Murshudov, G. N. Conformation-independent structural comparison of macromolecules with ProSMART. *Acta Crystallogr. D* **70,** 2487–2499 (2014).
59. Brown, A. *et al.* Tools for macromolecular model building and refinement into electron cryo-microscopy reconstructions. *Acta Crystallogr. D* **71,** 136–153 (2015).
60. Chen, V. B. *et al.* MolProbity: all-atom structure validation for macromolecular crystallography. *Acta Crystallogr. D* **66,** 12–21 (2010).
61. Schrodinger, LLC. The PyMOL Molecular Graphics System, Version 1.7. (2015).
62. Sievers, F. *et al.* Fast, scalable generation of high-quality protein multiple sequence alignments using Clustal Omega. *Mol. Syst. Biol.* **7,** 539 (2011).
63. Baker, N. A., Sept, D., Joseph, S., Holst, M. J. & McCammon, J. A. Electrostatics of nanosystems: application to microtubules and the ribosome. *Proc. Natl Acad. Sci. USA* **98,** 10037–10041 (2001).
64. Dolinsky, T. J., Nielsen, J. E., McCammon, J. A. & Baker, N. A. PDB2PQR: an automated pipeline for the setup of Poisson-Boltzmann electrostatics calculations. *Nucleic Acids Res.* **32,** W665–W667 (2004).
65. Jenner, L. B., Demeshkina, N., Yusupova, G. & Yusupov, M. Structural aspects of messenger RNA reading frame maintenance by the ribosome. *Nat. Struct. Mol. Biol.* **17,** 555–560 (2010).

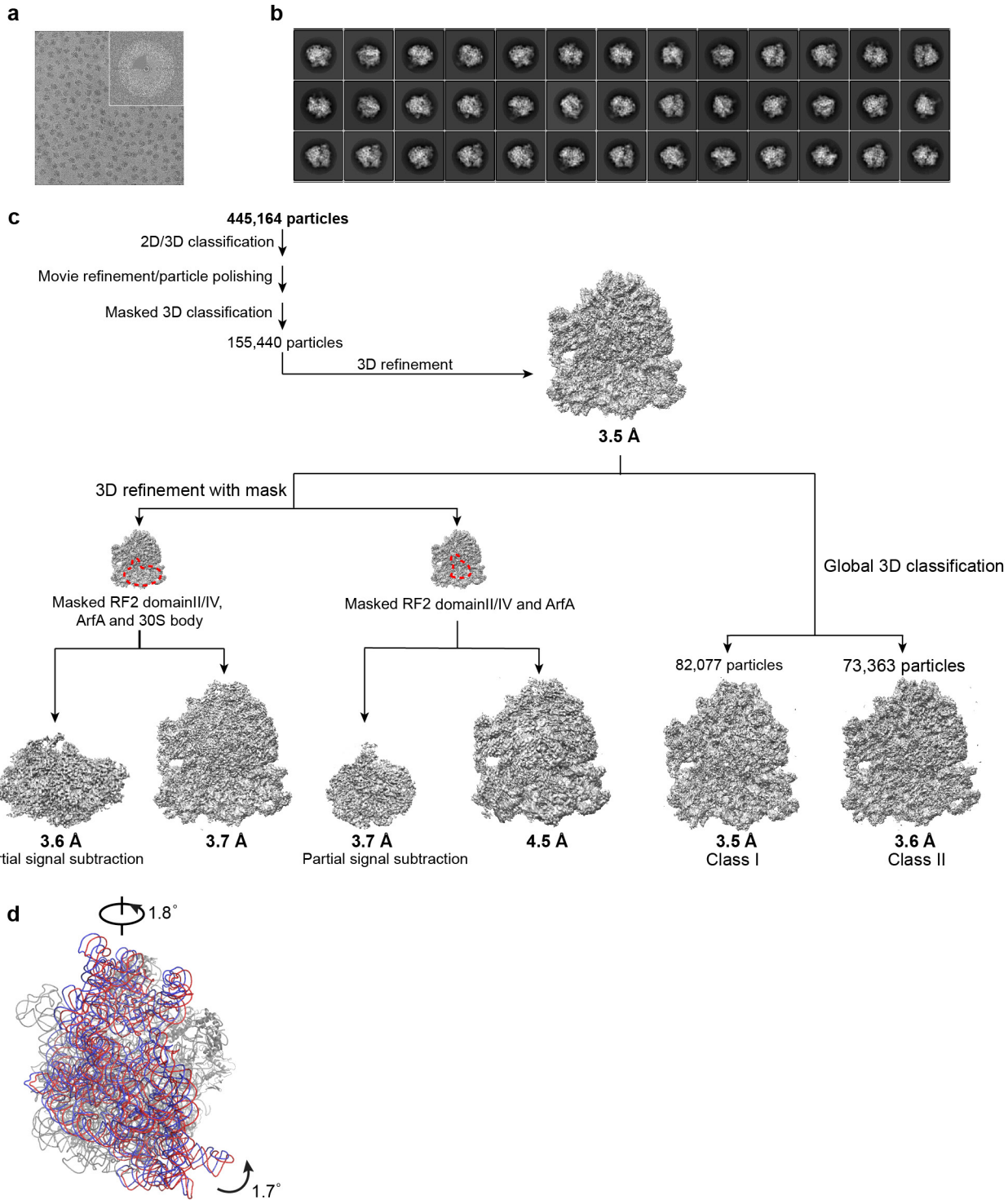

Extended Data Figure 1 | Structure determination of 70S ribosome with ArfA and RF2 on a nonstop mRNA by cryoEM. a, A representative micrograph with corresponding FFT shown in an insert. The insert shows the CTF estimation of an average background-subtracted power spectrum and fitted CTF (top-left corner) using CTFFIND4[40]. **b**, Representative 2D class averages from reference-free 2D classification. **c**, Particle classification and structural refinement procedures used to in this study. **d**, Conformational differences between the nonstop ribosomal complexes in the two classes obtained from the global classification and refinement. Rotation of 16S rRNA in the 30S subunit relative to 23S rRNA in the 50S subunit from class I (red) to class II (blue) showing a 1.7° 16S body domain rotation and an orthogonal 1.8° head domain rotation. Ribosomes in the two classes were aligned using the 23S rRNA of the 50S subunit. Small subunit ribosomal proteins are omitted for clarity.

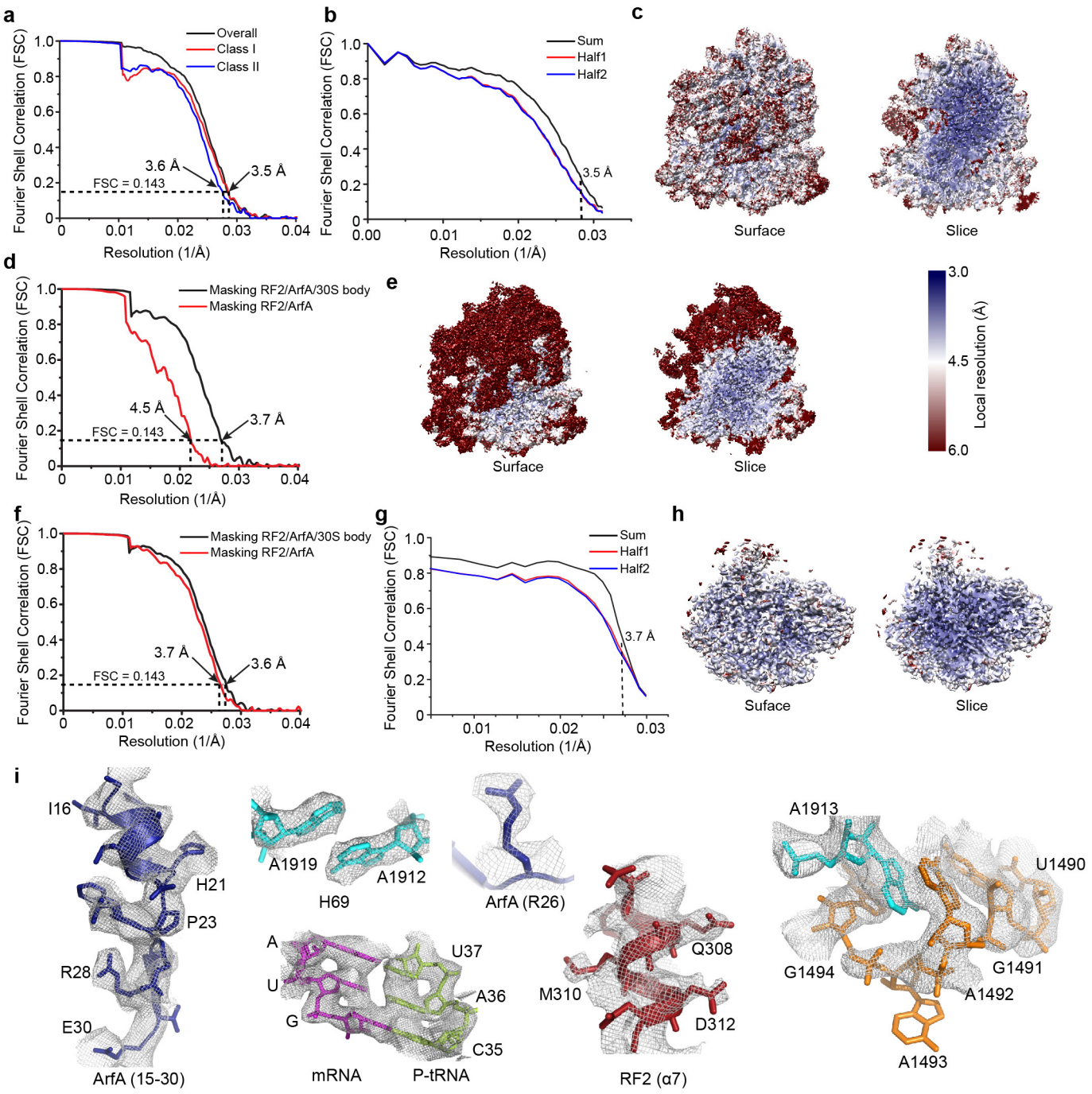

Extended Data Figure 2 | Map and model quality. a, Gold-standard FSC curves for the electron microscopy map from 155,440 particles (black), and electron microscopy maps of class I (red, 82,077 particles) and class II (blue, 73,363 particles) from the global 3D classification and refinement. Resolution is demarcated using the FSC = 0.143 criterion. **b**, Fit of the model to the map. FSC curves calculated between the refined structural model and the final electron microscopy map (sum, black), with the self-validated (half1, red) and cross-validated (half2, blue) correlations shown. **c**, The unfiltered and unsharpened density map coloured by local resolution in surface and slice views for the entire nonstop ribosomal complex. **d**, Gold-standard FSC curves for the electron microscopy maps obtained from the focused refinements with a mask over the ArfA/RF2/30S body domain (black) and a mask over the ArfA/RF2 region (red). **e**, Same as **c** for the electron microscopy map obtained from the focused refinement with a mask over the regions of ArfA, RF2 and the 30S body domain. **f**, Gold-standard FSC curves for the electron microscopy maps obtained from the local refinement with partial signal subtraction using a mask over the ArfA/RF2/30S body domain (black) and a mask over the ArfA/RF2 region (red). **g**, Fit of the model to the map. FSC curves are calculated between the refined structural model and the final electron microscopy map (sum, black) for the ArfA and RF2 region, with the self-validated (half1, red) and cross-validated (half2, blue) correlations shown. **h**, Same as **c** for the electron microscopy map obtained from the local refinement with a mask over the region of ArfA and RF2. **i**, Representative electron microscopy maps showing the refined structures of ArfA (density), RF2 (firebrick), 23S rRNA (cyan) and 16S rRNA (orange).

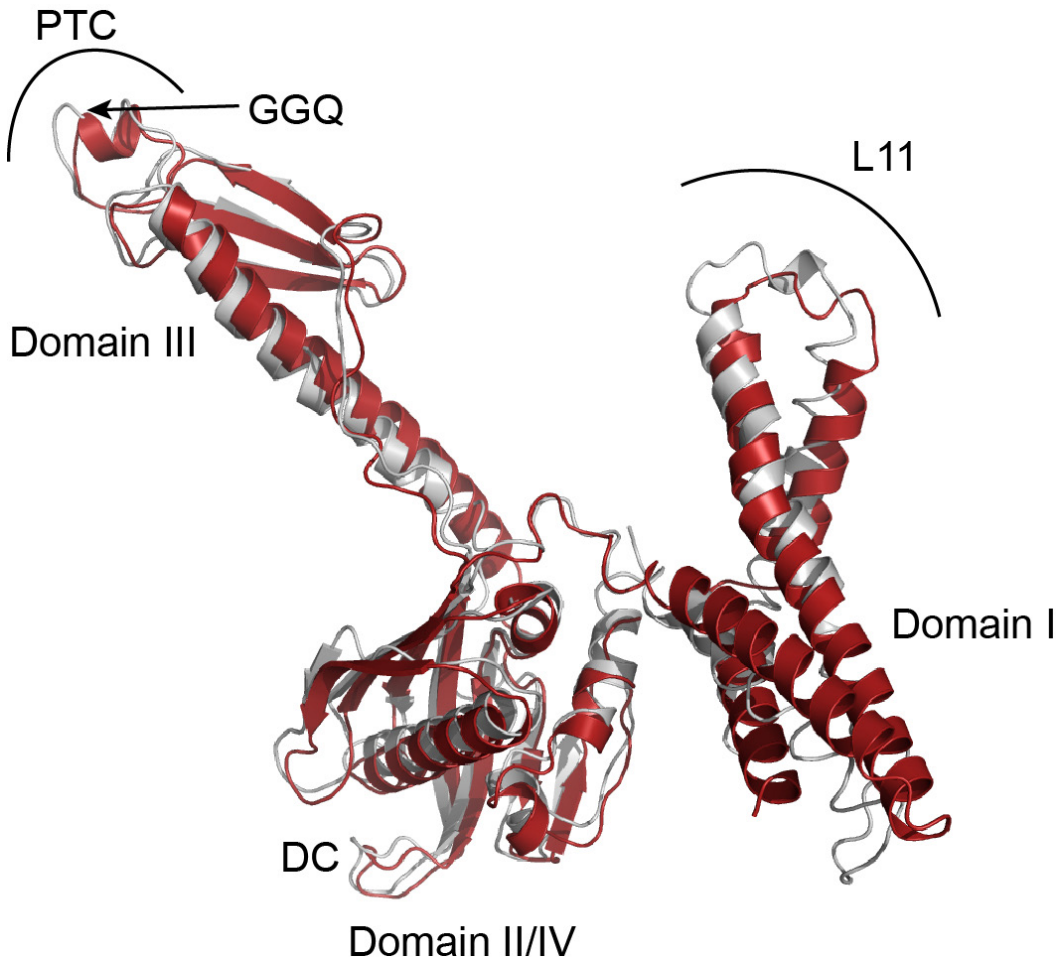

Extended Data Figure 3 | Conformations of RF2 in the canonical and nonstop termination complexes. Superposition of structures of RF2 in the canonical termination complex from *T. thermophilus* (PDB code: 4V5J[26], coloured in grey) and nonstop translation complex from *E. coli* (this study, coloured in red) based on an alignment of the 16S rRNAs of the two ribosomal complexes. In both structures, domains II and IV of RF2 bind to the decoding centre of the ribosome, domain III extends into the 50S subunit positioning the universally conserved GGQ motif into the PTC, and domain I interacts with the L11 stalk and the 30S shoulder region.

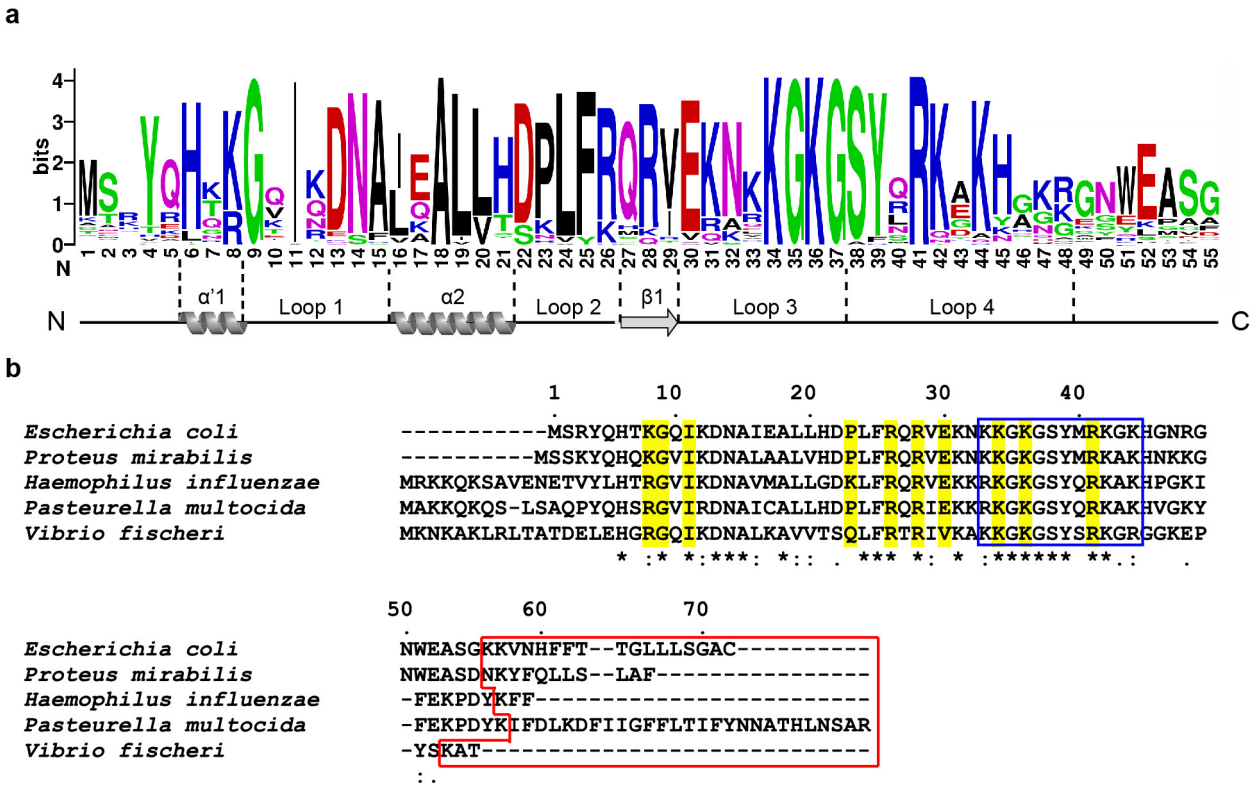

Extended Data Figure 4 | Sequence alignment of ArfA from different bacterial species. a, Pictorial representation of the consensus sequence showing the frequency of different amino acids in residues 1–55 of ArfA from 66 species. Alignment was generated by Weblogo (http://weblogo.berkeley.edu/logo.cgi), and amino acids are coloured according to their chemical properties. Polar and uncharged amino acids (G, S, T, Y, C) are coloured green, amino acids (Q, N) in purple, basic amino acids (K, R, H) in blue, acidic amino acids (D, E) in red, and hydrophobic amino acids (A, V, L, I, P, W, F, M) in black. Secondary structure features of ArfA from *E. coli* when it binds to the ribosome are shown according to the atomic structure obtained in this study. **b**, Multiple sequence alignment of ArfA proteins from different bacterial species showing that all ArfA proteins contain a positively charged C-terminal domain, as framed in the blue box. *E. coli* ArfA (NCBI GenInfo Identifier (GI) number 1450289), *Proteus mirabilis* ArfA (GI6802815), *Haemophilus influenza* ArfA (GI951152), *Pasteurella multocida* ArfA (GI29389120), and *Vibrio fischeri* ArfA (GI3280674) are used as examples. The red box indicates the C-terminal truncated region during ArfA maturation[17]. ArfA mutants used in this study are highlighted in yellow. Multiple sequence alignment was carried out in Clustal Omega[62].

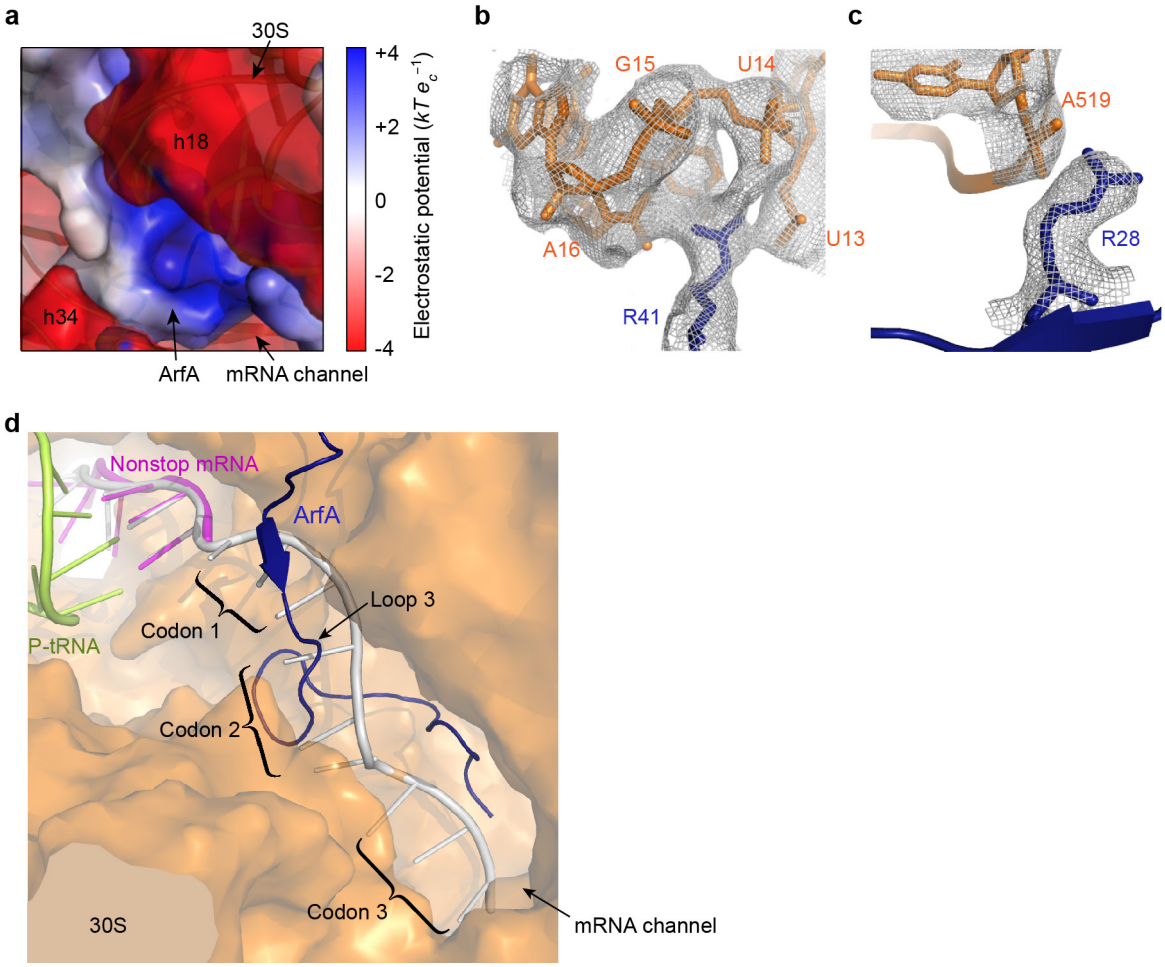

Extended Data Figure 5 | Interactions of the C-terminal tail of ArfA and the ribosome. a, View of the mRNA entry channel showing the positively charged residues in the C-terminal domain of ArfA interacting with negatively charged phosphate backbones of rRNA. RF2 is omitted for clarity. Electrostatic potentials were calculated using APBS[63] with pdb2pqr[64], where k is Boltzmann's constant, T is the system temperature of the calculation (310 K) and e_c is the charge of an electron. **b**, **c**, Positively charged residues in ArfA interact with phosphate backbones of the rRNA in the ribosome. Densities for selected ArfA residues are shown. R41 of ArfA makes contact with nucleotides in the mRNA entry channel (**b**). R28 of ArfA interacts with A519 of 16S rRNA (**c**). ArfA and16S rRNA are coloured blue and orange, respectively. **d**, Flexibility of loop 3 (E30–G37) in ArfA allows accommodation of a few nucleotides downstream from the P-site in the ribosome. One to two codons downstream of the ribosomal P-site appear to be accommodated by ArfA, and three codons downstream from the P-site nearly abolishes the peptide release activity in the ribosome, consistent with the biochemical data[1,4,13]. 30S is shown in yellow. ArfA, nonstop mRNA and P-tRNA are coloured in blue, magenta and lemon, respectively. An mRNA (grey) taken from PDB 4V6F[65] was used in the figure for the purpose of illustration.

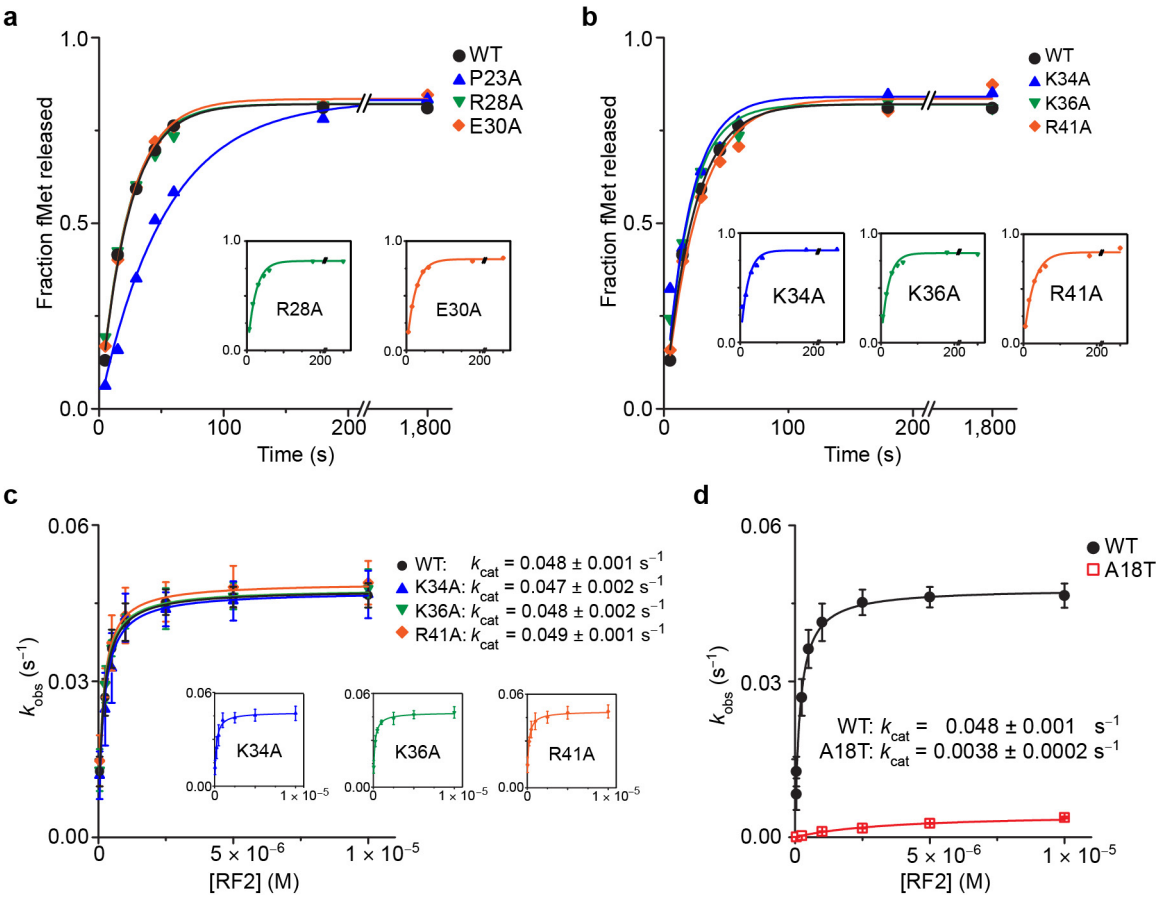

Extended Data Figure 6 | Peptide release by RF2 and ArfA mutants in the nonstop stalled ribosome. a, Representative time courses of peptide release for ArfA mutants with point mutations on residues interacting with the ribosomal decoding centre including P23A, R28A and E30A. **b**, Representative time courses of peptide release for ArfA mutants with point mutations in the C-terminal tail including K34A, K36A and R41A. Data on wild-type ArfA are shown. Ribosomal complexes (25 nM) with nonstop mRNA and P-site fMet-tRNA^{fMet} were incubated with 62.5 nM ArfA and 5 μM RF2 at 37 °C and the released peptides were measured at different time points after adding ArfA and RF2. **c**. Observed rate versus RF2 concentrations showing fits for k_{cat} and $K_{1/2}$ calculations for wild-type ArfA and K34A, K36A and R41A mutants. **d**, Observed rate versus RF2 concentrations showing fits for k_{cat} and $K_{1/2}$ calculations for wild-type ArfA and A18T mutant. The k_{cat} and $K_{1/2}$ values on A18T, $k_{cat} = 0.0038 \pm 0.0002\ s^{-1}$ and $K_{1/2} = 1.14 \pm 0.28 \times 10^{-6}$ M, were reported but the fitting curve was not shown[4]. k_{obs} was determined as described in Methods. Catalytic rate constants and values of $K_{1/2}$ were obtained by fitting the observed rates against the corresponding RF2 concentrations to the Michaelis–Menten equation. An average of three independent measurements is reported for each reaction and errors are calculated by standard error propagation.

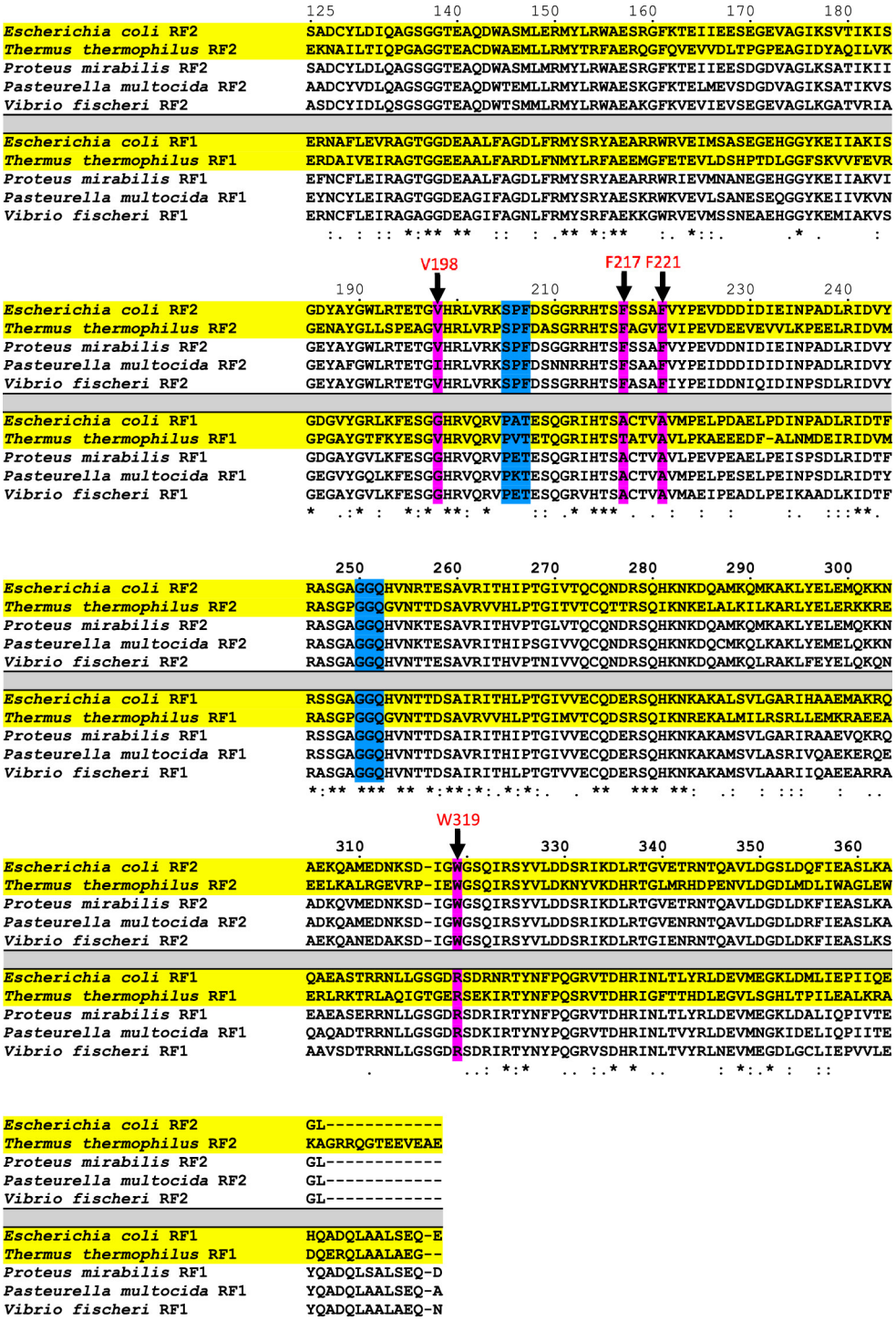

Extended Data Figure 7 | Multiple sequence alignment of domain II–IV of RF2 and RF1 from different bacterial species. *E. coli* RF1 (NCBI GenInfo Identifier number 949002) and RF2 (GI947369), *T. thermophilus* RF1 (GI3169506) and RF2 (GI3168831), *P. mirabilis* RF1 (GI6801441) and RF2 (GI23391224), *P. multocida* RF1 (GI29388454) and RF2 (GI29389590), and *V. fischeri* RF1 (GI3277422) and RF2 (GI3277319) were submitted to Clustal Omega for alignment. Except for the genome of *T. thermophiles*, which does not contain a gene for ArfA, the genomes of the other species all contain the *ArfA* gene[17]. The sequence alignment is validated by structural alignment of RF1 and RF2[22,25]. Domain I of RF1 and RF2 are omitted for clarity. The SPF and GGQ motifs are highlighted in cyan, and the four functionally important residues discussed in this study (V198, F217, F221 and W319) are highlighted in magenta. Sequences of RF1 and RF2 from *E. coli* and *T. thermophilus* are highlighted in yellow.

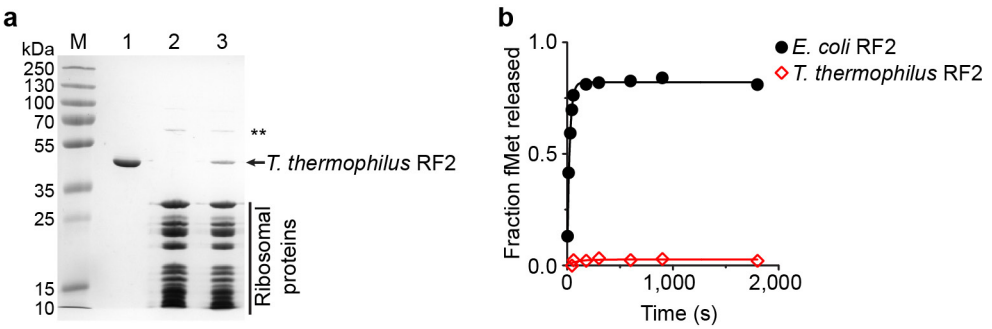

Extended Data Figure 8 | A heterologous ribosomal nonstop complex can be formed *in vitro* but is biologically inactive. a, RF2 from *T. thermophilus* binds to *E. coli* nonstop ribosomal complex *in vitro*. The heterologous nonstop ribosomal complex consisting of RF2 from *T. thermophilus* and ribosomes from *E. coli* was formed as described in Methods. SDS–PAGE shows *T. thermophilus* RF2 (lane 1), apo ribosome from *E. coli* (lane 2) and the formation of heterologous nonstop ribosomal complex after gel filtration (lane 3). **Ribosomal protein S1. **b**, The heterologous ribosomal complex fails to catalyse peptide release. Representative time courses of peptide release by 5 μM *E. coli* RF2 and *T. thermophilus* RF2 at 25 nM nonstop stalled ribosome and 62.5 nM ArfA from *E. coli* showing that *T. thermophilus* RF2 fails to catalyse peptide release in the ribosome.

Extended Data Table 1 | Data collection and model statistics

	Local refinement	Global refinement
Data Collection		
Particles	445,164	
Pixel size (Å)	0.5965	
Defocus range (μm)	-0.7 to -3.0	
Voltage (kV)	300	
Electron dose (e^{-}Å^{-2})	20	
Model composition		
Non-hydrogen atoms	11,368	149,529
Protein residues	521	6,100
RNA bases	494	4,715
Ligands (Zn^{2+}/Mg^{2+})	0/0	1/124
Refinement		
Resolution (Å)	3.7	3.5
Map sharpening B-factor (Å^2)	-50	-20
$FSC_{average}$	0.8424	0.7368
Rms deviations		
Bond lengths (Å)	0.0046	0.0051
Bond angles (°)	0.903	0.9606
Validation (proteins)		
Molprobity score	1.82 (100^{th})	2.61 (97^{th})
Clashscore, all atoms	2.86 (100^{th})	8.32 (97^{th})
Good rotamers (%)	97.18	90.96
Ramachandran plot		
Favored (%)	93.92	92.71
Outliers (%)	0.39	0.84
Validation (RNA)		
Correct sugar puckers (%)	96.46	98.68
Good backbone conformations (%)	78.31	70.24

Extended Data Table 2 | Rates and binding constants of peptide release for wild-type and mutants of ArfA on the nonstop ribosomal complex

ArfA	Ribosomal complex	k_{cat} (s^{-1})	$K_{1/2}$ (10^{-6} M)
	WT	0.048 ± 0.001*	0.16 ± 0.01*
C-terminal region (Residue 33-44)	K34A	0.047 ± 0.002	0.18 ± 0.02
	K36A	0.048 ± 0.002	0.15 ± 0.01
	R41A	0.049 ± 0.001	0.15 ± 0.01
Central region (Residue 23-30)	P23A	0.026 ± 0.001	0.25 ± 0.03
	R26A	0.047 ± 0.001	0.16 ± 0.03
	R28A	0.048 ± 0.001	0.15 ± 0.03
	E30A	0.048 ± 0.001	0.14 ± 0.02
Activation domain (Residue 1-18)	Δ18N	0.0037 ± 0.0002	1.04 ± 0.15
	K8A	0.013 ± 0.001	0.25 ± 0.07
	G9V	0.013 ± 0.001	0.26 ± 0.04
	I11N	0.0040 ± 0.0004	0.95 ± 0.21

*Catalytic rate constants k_{cat} and values of $K_{1/2}$ were obtained by fitting the observed rates against the corresponding RF2 concentrations to the Michaelis–Menten equation. An average of three independent measurements is reported for each reaction and errors are calculated by standard error propagation.